AIIM

Association for Information and Image Management

1100 Wayne Avenue, Suite 1100
Silver Spring, Maryland 20910

301/587-8202

Centimeter

Inches

MANUFACTURED TO AIIM STANDARDS
BY APPLIED IMAGE, INC.

PREPARED FOR THE U.S. DEPARTMENT OF ENERGY,
UNDER CONTRACT DE-AC02-76-CHO-3073

PPPL-2904
UC-420,427

PPPL-2904

GYROKINETIC SIMULATION OF ION TEMPERATURE GRADIENT DRIVEN TURBULENCE IN 3D TOROIDAL GEOMETRY

BY

S.E. PARKER, W.W. LEE AND R.A. SANTORO

MAY, 1993

PPPL PRINCETON PLASMA PHYSICS LABORATORY

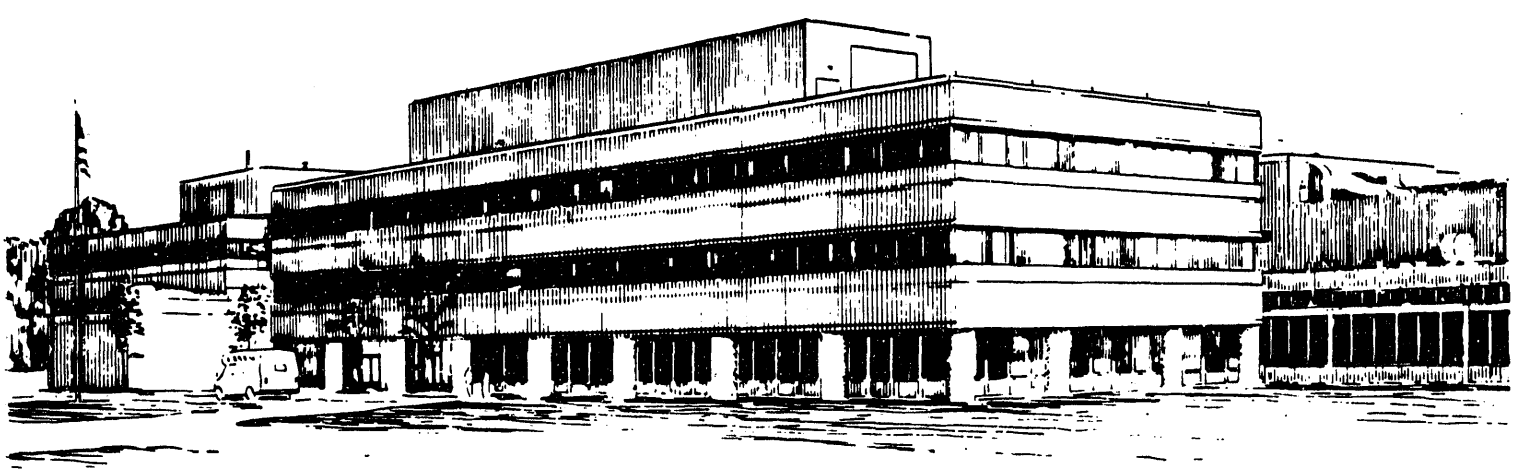

NOTICE

This report has been reproduced from the best available copy.
Available in paper copy and microfiche.

Number of pages in this report: 14

DOE and DOE contractors can obtain copies of this report from:

Office of Scientific and Technical Information
P.O. Box 62
Oak Ridge, TN 37831;
(615) 576-8401.

This report is publicly available from the:

National Technical Information Service
Department of Commerce
5285 Port Royal Road
Springfield, Virginia 22161
(703) 487-4650

Gyrokinetic Simulation of Ion Temperature Gradient Driven Turbulence in 3D Toroidal Geometry

S.E. Parker, W.W. Lee and R.A. Santoro

Princeton Plasma Physics Laboratory, Princeton University,
P.O. Box 451, Princeton NJ 08543

April 16, 1993

Abstract

Results from a fully nonlinear three dimensional toroidal electrostatic gyrokinetic simulation of the ion temperature gradient instability are presented. The model has fully gyro-averaged ion dynamics, including trapped particles, and adiabatic electrons. Simulations of large tokamak plasma volumes are made possible due to recent advances in δf methods and massively parallel computing. Linearly, a coherent ballooning eigenmode is observed, where the mode is radially elongated. In the turbulent steady-state, the spectrum peaks around $k_\theta \rho_s \sim 0.1 - 0.2$ and $k_r \rho_s \sim 0$, with the ballooning structure reduced, but still prevalent.

1 Introduction

Recent advances in both nonlinear δf methods for gyrokinetic simulation [1, 2], and massively parallel supercomputing now make it possible to simulate a sizable fraction of a tokamak plasma using realistic physical parameters. As a first step in utilizing these advances, a three dimensional electrostatic toroidal gyrokinetic simulation has been developed. Here, the code is used to investigate the nonlinear evolution of the ion temperature gradient (ITG) driven instability and the associated turbulence and transport. The ITG mode has long been considered a plausible candidate to explain the anomalous ion heat transport above neoclassical values in tokamak plasmas [3, 4].

In these simulations, the ions are fully gyrokinetic, including trapped particles. The electrons are treated as adiabatic which permits a moderate size timestep (simulations with kinetic electrons are feasible, but the timestep would need to be smaller by the factor v_{te}/v_{ti}). The simulation is efficiently running on massively parallel supercomputers (currently the CM-200 and CM-5) which allows simulations of relatively large systems (e.g., $a \gtrsim 100\rho_i$ minor radius, $\Delta x \approx \rho_i$). Typical runs up to this point have ranged from one to *eight million particles* and grid cells usually with one to two particles per grid cell, and with a cpu time of 2-3 microseconds per particle per timestep on a full 64K processor CM200. Fine grid resolution is needed in the toroidal direction because the mode structure is the helical (elongated along the the magnetic field lines i.e., $k_\parallel \ll k_\perp$), resulting in a smaller number of particles per grid cell relative to conventional slab simulations.

In the initial phase of the run, we observe a clean linear growth of the most unstable toroidal harmonic and the associated 2D eigenmode in (r, θ) with a ballooning type structure where the mode is radially elongated. [Fig. 1 (a) and (b)]. In the steady-state, both long and short perpendicular wavelengths are enhanced with the spectrum peaking at $k_r\rho_s \sim 0$ and $k_\theta\rho_s \sim 0.1 - 0.2$, and the ballooning structure reduced, but still prevalent [Fig. 1 (d) and (e)]. Broad scale (i.e., many modes are present) turbulence with fluctuation levels of $e|\phi_k|/T \lesssim 1\%$ is observed. The parameters and more details will be given in Sec. 3, where it will be shown that the k_r and k_θ spectrum (Fig. 3) show very similar features as the the recent beam emission spectroscopy (BES) fluctuation measurements on TFTR [5].

2 Model Equations

Starting with the electrostatic gyrokinetic equations with a nonuniform equilibrium B-field [6], we write $f(\mathbf{z},t) = f_0(\mathbf{z}) + \delta f(\mathbf{z},t)$, where $\mathbf{z} = (\mathbf{R}, v_\parallel, \mu)$; and expand $\dot{\mathbf{z}}$ into its equilibrium and perturbed parts: $\dot{\mathbf{z}} = \dot{\mathbf{z}}^0 + \dot{\mathbf{z}}^1$. $f_0(\mathbf{z})$ is a Maxwellian and satisfies: $\dot{\mathbf{z}}^0 \cdot \partial_{\mathbf{z}} f_0(\mathbf{z}) = 0$. The equation for the perturbed ion distribution function δf is then [1]

$$\partial_t \delta f + \dot{\mathbf{z}} \cdot \partial_{\mathbf{z}} \delta f = -\dot{\mathbf{z}}^1 \cdot \partial_{\mathbf{z}} f_0. \tag{1}$$

where the magnetic moment μ is time independent and the other equilibrium and perturbed phase space variables are evolved using

$$\left(\dot{\mathbf{R}}^0, \dot{v_\parallel}^0\right) = \left(-v_\parallel \hat{\mathbf{b}}^* + \frac{\mu}{B}\hat{\mathbf{b}} \times \nabla B, \hat{\mathbf{b}}^* \cdot \mu \nabla B\right), \tag{2}$$

$$\left(\dot{\mathbf{R}}^1, \dot{v_\parallel}^1\right) = \left(\frac{\hat{\mathbf{b}}}{B} \times \nabla\bar{\phi}, -\hat{\mathbf{b}}^* \cdot \nabla\bar{\phi}\right), \tag{3}$$

where $\hat{\mathbf{b}}^* \equiv \hat{\mathbf{b}} + \frac{v_\parallel}{B}\hat{\mathbf{b}} \times \hat{\mathbf{b}} \cdot \nabla\hat{\mathbf{b}}$, $\bar{\phi}$ is the gyro-averaged electrostatic potential, and dimensionless gyrokinetic units are used $R/\rho_s \to R$, $v_\parallel/c_s \to v_\parallel$, $e\bar{\phi}/T_e \to \bar{\phi}$, $\Omega_i t \to t$, $B/B_0 \to B$, B_0 is a reference value of B, $\mu = (v_\perp/c_s)^2/(2B/B_0)$, $\Omega_i = eB_0/(m_i c)$, $c_s = \sqrt{T_e/m_i}$, and $\rho_s = c_s/\Omega_i$.

The particles follow their full nonlinear trajectories, δf is represented by $B\delta f(\mathbf{z},t) = \sum_i w_i \delta(\mathbf{z} - \mathbf{z}_i)$, and particle weight w_i is then evolved using [1]

$$\dot{w}_i = -(1 - w_i)\left[\dot{\mathbf{z}}^1 \cdot \frac{\partial_{\mathbf{z}} f_0}{f_0}\right]_{\mathbf{z}=\mathbf{z}_i,t}. \tag{4}$$

Electromagnetic equations have been formulated [1], but not yet implemented in the code. Equations (2)-(3) are similar to those of Hahm's [6], and accurate to the same order but, we have assumed $B^* = B$ for numerical efficiency. As usual, finite size particles are used in the configuration space. The electrons are are assumed adiabatic

($\delta n_e = n_0 e\phi/T_e$). A square cross-section is used which is suitable for spectral solution of the field equation. The coordinates (x, y, ψ) in terms of the usual toroidal coordinates (r, θ, ψ) are: ($x = r\cos\theta, y = r\sin\theta, \psi$). Using these coordinates, assuming $(k_{\|}/k_{\perp})(B_\theta/B_\psi) \ll 1$ where B_θ and B_ψ are the poloidal and toroidal components of $\mathbf{B}$, one can transform the electrostatic field equation [7] to obtain:

$$\tau[1 - \Gamma_0(\mathbf{k}_\perp^2/T_i/T_e)]\phi(\mathbf{k}_\perp, \psi) = \delta\bar{n}_i(\mathbf{k}_\perp, \psi) - \phi(\mathbf{k}_\perp, \psi), \quad (5)$$

where $\delta\bar{n}_i = (\bar{n}_i - n_0)/n_0$, $\bar{n}_i$ is the gyro-averaged ion density, $\mathbf{k}_\perp = (k_x\rho_s, k_y\rho_s)$ and higher order terms have been neglected. ρ_s is assumed constant in Eq. (5). For the radial boundary condition we set $\delta\bar{n}_i$ to zero for $r \geq (a - 4\rho_s)$ within the square cross-section. The magnetic field is fixed and specified using $B_\psi = B_0 R_0/R$, $B_\theta = rB_\psi/(R_0 q(r))$, and $q(r) = q_0 + \Delta q(r/a)^2$. Initial equilibrium density and temperature profiles are used such that $L_n^{-1} \equiv |\nabla n|/n$ and $L_T^{-1} \equiv |\nabla T|/T$ have a radial variation proportional to $\mathrm{sech}^2[(r - r_0)/l]$, where r_0 and l as well as the peak normalized gradients $L_n^{-1}(r_0)$ and $L_T^{-1}(r_0)$ are all specified parameters. For the results presented, the particles are loaded homogeneously and the variation in the profile appears only in the right hand side of Eq. (4).

3 Simulation Results

The results shown here are for a run using the following numerical parameters: 1 million particles, a 128x128x64 grid in (x, y, ψ), with a perpendicular grid cell size $\Delta x = \Delta y = \rho_s$, and a time step of $\Delta t c_s/L_T = 0.45$. The physical parameters are: $\epsilon_T \equiv L_T(r_0)/R_0 = 0.075$, $1/L_n(r_0) = 0$, $T_i = T_e$, $a = 64\rho_s$, and $R_0 = 892\rho_s$, $q_0 = 1.25$, $\Delta q = 3$, $l = 20\rho_s$, $r_0 = \frac{1}{2}a$ is the location of maximum temperature gradient (see Sec. 2), $q(r_0) = 2$, $\hat{s} \equiv \dfrac{r}{q}\dfrac{dq}{dr} = 0.75$ at r_0. The local parameters at $r = r_0$ are similar to the TFTR perturbed supershot experiment [8], except for the aspect ratio. As mentioned above Figures 1(a) and (b) are the poloidal and toroidal slices of the potential in the linear phase. Figure 1(c) shows the relative amplitude of the various (m, n) modes in the linear phase at the $q(r=\frac{1}{2}a)=2$ flux surface for $\phi = \sum_{m,n} \phi_{mn} \exp(-im\theta - in\psi)$. One dominant toroidal harmonic is present ($n=4$) with a dominant poloidal harmonic ($m=8, k_\theta = m/r_0 = 0.25$) plus a few lower amplitude sidebands to produce the ballooning envelope. Figures 1(a)-(e) are snapshots taken just before the saturation of the dominant mode.

The measured real frequency is $\omega_r = -0.06 c_s/L_T$ and the growth rate is $\gamma = 0.03 c_s/L_T$. The closest analytic theory for toroidal ITG modes in terms of the assumed ordering is the slab branch in the long wavelength limit[4] with $\omega \sim \omega_{ti} \sim \epsilon_T^{1/2} \omega_{*Ti}$, $k_\theta \rho_i \sim \epsilon_T^{1/2}$, $\Delta\theta \sim \epsilon_T^{-1/4}$, where $\Delta\theta$ is the mode width in the extended poloidal angle; and the approximate dispersion relation given by

$$\omega = \frac{v_{ti}}{qR_0}(7\sqrt{\pi})^{1/5}\left[(qk_\theta\rho_s)^2\hat{s}/\epsilon_T\right]^{(2/5)} e^{i7\pi/10}, \tag{6}$$

which gives $\omega_r = -0.05 c_s/L_T$ and $\gamma = 0.07 c_s/L_T$. Comparisons with more detailed eigenmode calculations of Rewoldt and Tang [3] show agreement is within 15% in terms of real frequency, growth rate, and mode structure [9]. This dominant eigenmode grows linearly and saturates at a level of $e|\phi(r=r_0, \theta=0, n=4)|/T_e = 0.03$, which is in the range of the mixing length level $1/(k_\perp L_T) = 0.06$, where we used L_T since $1/L_n = 0$ and $k_\perp \approx k_\theta$. The local shearless slab mode coupling calculation of Lee and Tang [10] predicts a saturation level $e/T_e|\phi(x)| = \sqrt{3}|\omega + i\gamma|/k_\perp^2 \approx 0.03$, which is in agreement with the toroidal simulation result. This may be due to the fact that the radially elongated mode structure is not strongly localized by the magnetic shear. Toroidal effects on the mode coupling calculation will be investigated in the future. At saturation, $\chi_i = 1.6\rho_s^2 c_s/L_T$ taken at $r = r_0$, then drops and comes to a steady-state value of $\chi_i = 0.2\rho_s^2 c_s/L_T$, for comparison $\gamma/k_\perp^2 = 0.5\rho_s^2 c_s/L_T$, again using $k_\perp \approx k_\theta$.

Figures 1(d)-(f) are the corresponding plots during the nonlinear saturated steady-state. These snapshots were taken at a time $300 L_T/c_s$ after the saturation of the fastest growing mode. Figures 1(c) and (f) show that the poloidal and toroidal harmonics (m, n) have appreciable activity for the linear phase and the nonlinear state, respectively. After the system settles down to a steady-state, the activity is at a lower (m, n) than the (m, n) associated with the most unstable mode. We also note that the peak of activity lies on the $m = qn$ line as expected. Figures 2(a) and (b) are the k_θ and k_r spectrum taken at the turbulent stead-state. These measurements were made over the half annular region of $\theta \in [-\pi/2, +\pi/2]$, $r \in [\frac{1}{4}a, \frac{3}{4}a]$ and $\psi \in [-\pi, \pi]$. The region has approximately a $32\rho_s$ $(= a/2)$ radial width and a $100\rho_s$ $(= \pi a/2)$ poloidal length. Figure 2(a) shows $S(k_\theta) \equiv \sum_{n,k_r} |\phi(k_r, k_\theta, n)|^2$. and Fig. 2(b) shows $S(k_r) \equiv \sum_{n,k_\theta} |\phi(k_r, k_\theta, n)|^2$, These diagnostics are an attempt at mimicking the recent BES measurements on TFTR [5]. The spectrum shows similar features as the experimental measurements in that the k_r spectrum peaks at zero and k_θ spectrum peaks in the range of $k_\theta \rho_s \sim$ 0.1-0.2. These properties of the spectrum have so far been found to be fairly insensitive to the choice of simulation parameters. One notable difference between the numerical result and the experimental measurement is that the width in the in the k_r spectrum is broader in the simulation. One possible explanation is the small minor radius of the simulation causes more localization of the modes radially, hence artificially broadening the k_r spectrum. This will be tested in the future, as the size of the simulations can be increased.

Figure 3(a) shows the initial temperature profile (solid line) and the flattened profile in the quasi-steady state(dashed line). The dashed line is measured at a time $750 L_T/c_s$ past the saturation of the most unstable mode, at which time the center temperature has dropped by 8%. We use the term quasi-steady-state because the profile continues to relax due to diffusion, but on a much slower timescale than the initial transients and the ensuing fluctuations. Figure 3(b) shows the radial variation in χ_i, which appears fairly flat, except towards the edge where χ_i goes to zero because the ion density fluctuations are set to zero in the simulation for $r \geq (a - 4\rho_i)$. Simulations with larger volumes will probably be needed to compare with the experimentally observed trends in the $\chi_i(r)$ profile. The peak (and overall) level is approximately $\chi_i \approx 0.2\rho_s^2 c_s/L_T$ [Fig. 3(b)]. We have also run a case with the same parameters *except* for using a finite L_n, such that $\eta_i = L_T/L_n = 2.3$, the purpose being to see the effect of running closer to marginal stability and compare with the unperturbed supershot parameters [8]. In $\eta_i = 2.3$ case, the steady-state χ_i is reduced to approximately $0.06\rho_s^2 c_s/L_T$.

Though, not identical parameters (e.g., T_e/T_i is held fixed for both simulation cases), and simplified physics it is interesting to compare the simulation results to the thermal diffusivity in gyro-Bohm units for the perturbation experiment on TFTR [8], where for both the perturbed and unperturbed case $\chi_i \approx 0.3\rho_s^2 c_s/L_T$. In comparison, the simulation shows a considerable reduction in the gyro-Bohm coefficient for the case closer to marginal stability ($\eta_i = 2.3$). This discrepency may be in part due simplified physics model. Effects that have been found to play an important role in linear calculations, but are not in our nonlinear model include trapped electrons, collisions, energetic ions, and impurities [11, 12, 13]. Also, collisions have been shown to have a significant effect on the steady-state fluxes in nonlinear gyrokinetic simulations [10].

To gain some insight of the scaling trends of ITG driven transport, one can examine the invariance properties [14] of the governing equations. In the gyrofluid limit, the scaling can be written as [10]

$$\chi_i \propto (k_\perp \rho_s)^{-p}(\rho_s/L_T)(cT/eB), \tag{7}$$

using $k_\parallel \approx 1/qR$ and $L_T/R = const$. Although the quasilinear theory gives $p = 5/3$ [10], in general, the exponent p does not have a unique solution (because of the insufficient number of allowable transformations). Nevertheless, this scaling indicates that, if $k_\perp \rho_s$ spectrum in the turbulent steady state remains unchanged for different sizes of minor radius, a, the magnitude of χ_i should remain constant, which would give gyro-Bohm scaling. However, preliminary indications from larger simulations show that χ_i increases with system size. Thus, the scaling is not entirely gyro-Bohm. Furthermore, the simulation has a minor radius which is 5-10 times smaller, in comparison with the TFTR experiments [5, 8], and has a wider k_r spectrum and a smaller χ_i. This is a signature of non-gyro-Bohm scaling and the trend is consistent with Eq. (7).

4 Discussion

Results from a three dimensional toroidal electrostatic gyrokinetic simulation were presented. A coherent ballooning eigenmode is observed in the initial linear phase. This dominant mode first saturates, then a turbulent steady-state develops, in which the k_r and k_θ spectrums show similar features as the recent BES measurements on TFTR. We have demonstrated the feasibility of using large scale gyrokinetic simulations to study the nonlinear evolution of kinetic microinstabilities. Current whole tokamak simulations are limited to minor radii of 100-200ρ_s. In the future, teraflop scale massively parallel supercomputers will allow simulations with a minor radius in the range of 400ρ_s, which is typical of the size of present day tokamaks. Such simulations can serve as a useful tool for better understanding of tokamak turbulence. In the interim, it may also be possible to simulate a reduced volume such as an annulus or flux tube. However, using smaller domains typically require more assumptions to be made about the underlying mode structure and/or turbulence. Global kinetic simulations such as these presented here should help identify, as well as, verify such simplified models. Future work will include adding a more detailed kinetic electron model (including the trapped fraction), electromagnetic perturbations, and collisional effects.

Acknowledgments

We thank L. Chen, J. Li, H.E. Mynick, G.W. Rewoldt, J.V. Reynders, W.M. Tang and X.Q. Xu for helpful discussions. Computer resources where provided by the Advanced Computer Laboratory, Los Alamos National Laboratory. Work supported by the U.S. Department of Energy Contract No. DE-AC02-76-CHO-3073.

References

[1] S.E. Parker and W.W. Lee, Phys. Fluids B **5** 77 (1993).

[2] A.M. Dimits and W.W. Lee, to appear in J. Comput. Phys.

[3] W.M. Tang and G. Rewoldt, to appear Phys. Fluids B 1993.

[4] F. Romanelli, L. Chen and S. Briguglio, Phys. Fluids B **3** 2496 (1991).

[5] R. Fonck, N. Bretz, G. Cosby, R. Durst, E. Mazzucato, R. Nazikian, S. Paul, S. Scott, W.Tang, and M. Zarnstorff, Plasma Phys. **32** 1993 (1992).

[6] T.S. Hahm, Phys. Fluids **31** 2670 (1988).

[7] W.W. Lee, J. Comput. Phys. **72**, 243 (1987).

[8] M.C. Zarnstorff, N.L. Bretz, P.C. Efthimion, B. Grek, K. Hill, D. Johnson, D. Mansfield, D. McCune, D.K. Owens, H. Park, A. Ramsey, G.L. Schmidt, B. Stratton, E. Synakowski, and G.Taylor, Proc. of the 13th Int. Conf. on Plasma Phys. and Contr. Nucl. Fus. Res., Washington D.C., 1990, Vol. 1, p. 39.

[9] S.E. Parker, R.A. Santoro and W.W. Lee, Bull. Am. Phys. Soc. **37** 1554 (1992).

[10] W.W. Lee and W.M. Tang, Phys. Fluids, **31** 612 (1988).

[11] G. Rewoldt and W.M. Tang, Phys. Fluids B, **2** 318 (1990).

[12] X.Q. Xu and M.N. Rosenbluth, Phys. Fluids B **3** 627 (1991).

[13] M. Kotschenruether, Bull. Am. Phys. Soc. **37** 1432 (1992).

[14] J.W. Connor and J.B. Taylor, Nucl. Fusion, **17** 1047 (1977).

Figures

Figure 1: Plots of the electrostatic potential during the linear phase and nonlinearly saturated steady-state. (a) poloidal cross-section during the linear phase, (b) toroidal cross-section during the linear phase, (c) excited toroidal and poloidal harmonics during the linear phase, the size of the circle indicates amplitude of the potential, measurement is made at the $q = 2$ surface; (d)-(f) are the same diagnostics, taken during the saturated steady-state.

Figure 2: Wavelength fluctuation spectrum for k_θ and k_r. (a) Fluctuation amplitude vs. k_θ, and (b) fluctuation amplitude vs. k_r. k_r and k_θ are in units of ρ_s^{-1}, and S is in arbitrary units.

Figure 3: Radial temperature profile and heat diffusivity. (a) Temperature vs. radius, initial equilibrium is the solid line, dashed line is the steady-state; (b) heat diffusivity χ_i vs. radius at steady-state, the solid line is χ_i calculated using initial equilibrium and the dashed line is calculated using the evolved equilibrium.

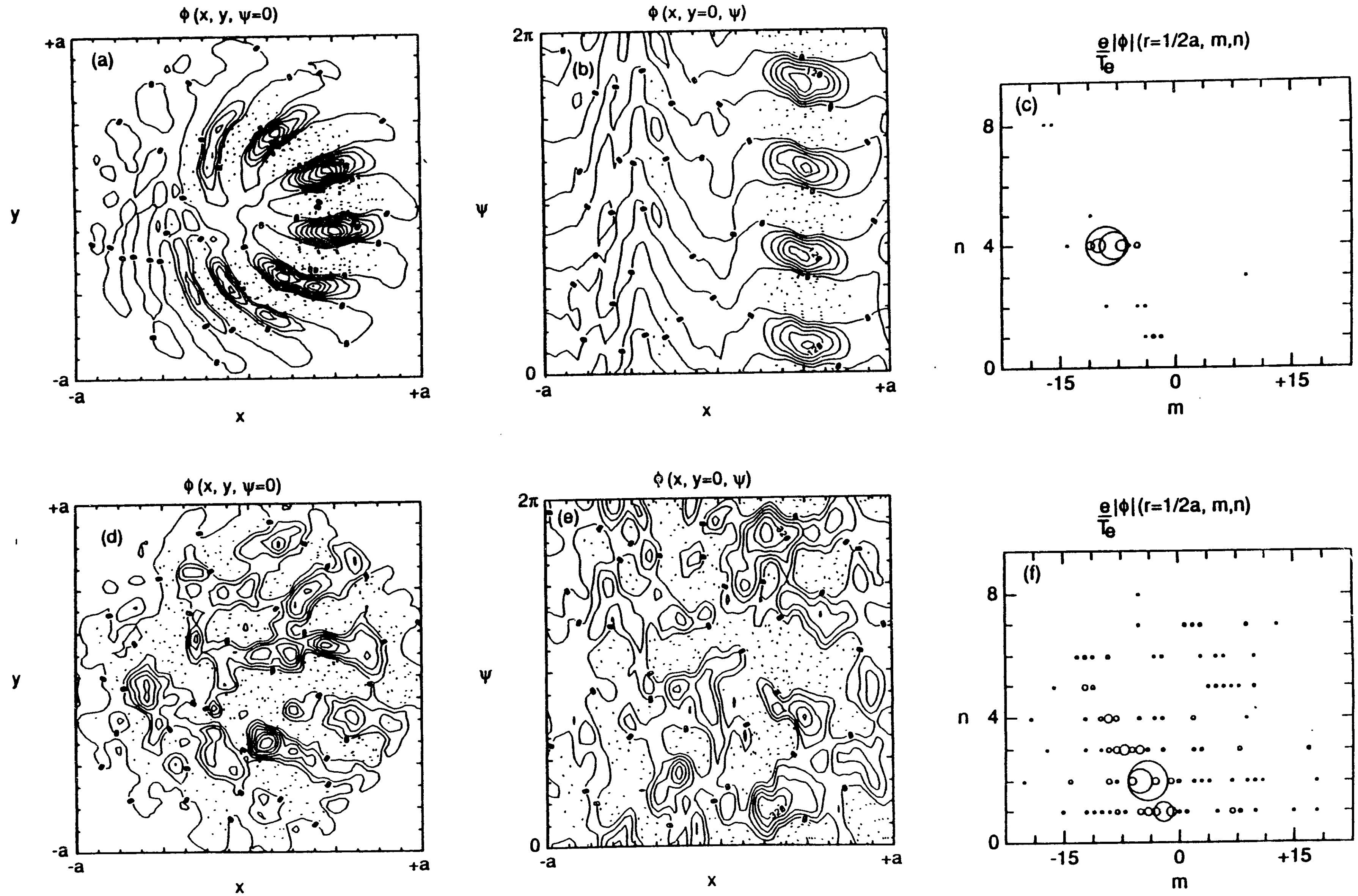

φ (x, y, ψ=0)
(a)
+a
-a
y
x
φ (x, y=0, ψ)
(b)
2π
0
ψ
x
e/Te |φ|(r=1/2a, m,n)
(c)
n
m
-15
0
+15
8
4
φ (x, y, ψ=0)
(d)
φ (x, y=0, ψ)
(e)
e/Te |φ|(r=1/2a, m,n)
(f)

Fig. 1 (a)-(f)

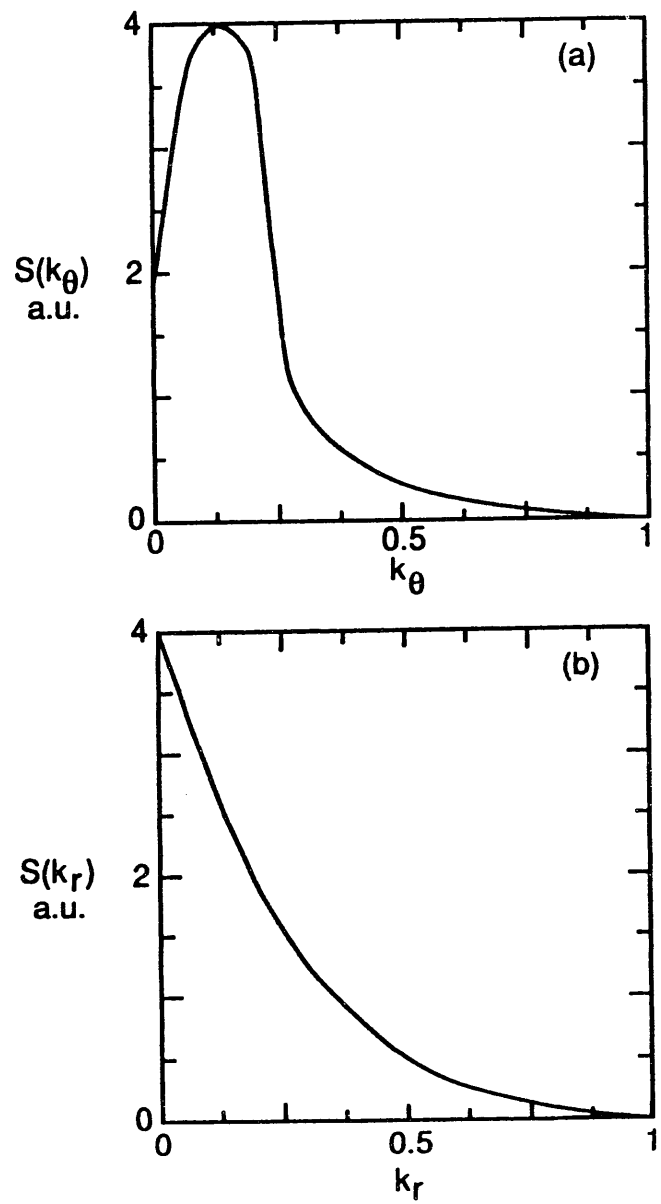

Fig. 2 (a) and (b)

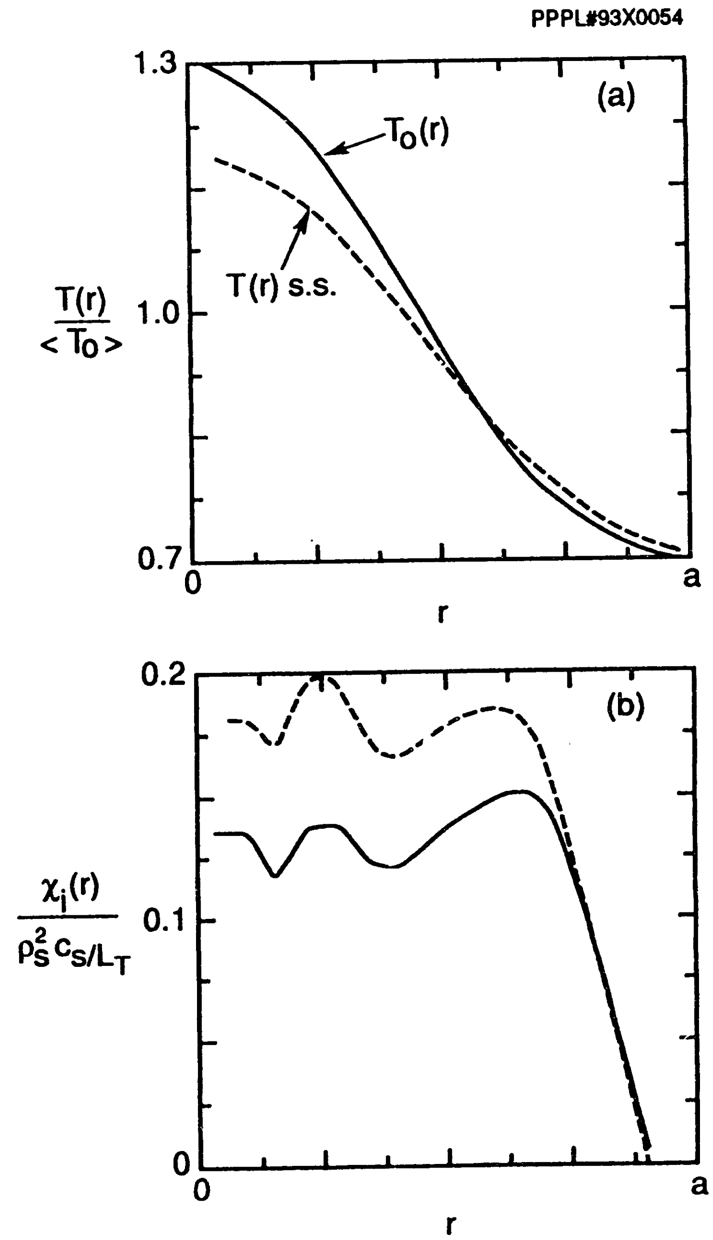

Fig. 3 (a) and (b)

EXTERNAL DISTRIBUTION IN ADDITION TO UC-420

Dr. F. Paoloni, Univ. of Wollongong, AUSTRALIA
Prof. M.H. Brennan, Univ. of Sydney, AUSTRALIA
Plasma Research Lab., Australian Nat. Univ., AUSTRALIA
Prof. I.R. Jones, Flinders Univ, AUSTRALIA
Prof. F. Cap, Inst. for Theoretical Physics, AUSTRIA
Prof. M. Heindler, Institut für Theoretische Physik, AUSTRIA
Prof. M. Goossens, Astronomisch Instituut, BELGIUM
Ecole Royale Militaire, Lab. de Phy. Plasmas, BELGIUM
Commission-European, DG. XII-Fusion Prog., BELGIUM
Prof. R. Bouciqué, Rijksuniversiteit Gent, BELGIUM
Dr. P.H. Sakanaka, Instituto Fisica, BRAZIL
Instituto Nacional De Pesquisas Espaciais-INPE, BRAZIL
Documents Office, Atomic Energy of Canada Ltd., CANADA
Dr. M.P. Bachynski, MPB Technologies, Inc., CANADA
Dr. H.M. Skarsgard, Univ. of Saskatchewan, CANADA
Prof. J. Teichmann, Univ. of Montreal, CANADA
Prof. S.R. Sreenivasan, Univ. of Calgary, CANADA
Prof. T.W. Johnston, INRS-Energie, CANADA
Dr. R. Bolton, Centre canadien de fusion magnétique, CANADA
Dr. C.R. James,, Univ. of Alberta, CANADA
Dr. P. Lukác, Komenského Universzita, CZECHO-SLOVAKIA
The Librarian, Culham Laboratory, ENGLAND
Library, R61, Rutherford Appleton Laboratory, ENGLAND
Mrs. S.A. Hutchinson, JET Library, ENGLAND
Dr. S.C. Sharma, Univ. of South Pacific, FIJI ISLANDS
P. Mähönen, Univ. of Helsinki, FINLAND
Prof. M.N. Bussac, Ecole Polytechnique,, FRANCE
C. Mouttet, Lab. de Physique des Milieux Ionisés, FRANCE
J. Radet, CEN/CADARACHE - Bat 506, FRANCE
Prof. E. Economou, Univ. of Crete, GREECE
Ms. C. Rinni, Univ. of Ioannina, GREECE
Dr. T. Mual, Academy Bibliographic Ser., HONG KONG
Preprint Library, Hungarian Academy of Sci., HUNGARY
Dr. B. DasGupta, Saha Inst. of Nuclear Physics, INDIA
Dr. P. Kaw, Inst. for Plasma Research, INDIA
Dr. P. Rosenau, Israel Inst. of Technology, ISRAEL
Librarian, International Center for Theo Physics, ITALY
Miss C. De Palo, Associazione EURATOM-ENEA , ITALY
Dr. G. Grosso, Istituto di Fisica del Plasma, ITALY
Prof. G. Rostangni, Istituto Gas Ionizzati Del Cnr, ITALY
Dr. H. Yamato, Toshiba Res & Devel Center, JAPAN
Prof. I. Kawakami, Hiroshima Univ., JAPAN
Prof. K. Nishikawa, Hiroshima Univ., JAPAN
Director, Japan Atomic Energy Research Inst., JAPAN
Prof. S. Itoh, Kyushu Univ., JAPAN
Research Info. Ctr., National Instit. for Fusion Science, JAPAN
Prof. S. Tanaka, Kyoto Univ., JAPAN
Library, Kyoto Univ., JAPAN
Prof. N. Inoue, Univ. of Tokyo, JAPAN
Secretary, Plasma Section, Electrotechnical Lab., JAPAN
S. Mori, Technical Advisor, JAERI, JAPAN
Dr. O. Mitarai, Kumamoto Inst. of Technology, JAPAN
J. Hyeon-Sook, Korea Atomic Energy Research Inst., KOREA
D.I. Choi, The Korea Adv. Inst. of Sci. & Tech., KOREA
Prof. B.S. Liley, Univ. of Waikato, NEW ZEALAND
Inst of Physics, Chinese Acad Sci PEOPLE'S REP. OF CHINA
Library, Inst. of Plasma Physics, PEOPLE'S REP. OF CHINA
Tsinghua Univ. Library, PEOPLE'S REPUBLIC OF CHINA
Z. Li, S.W. Inst Physics, PEOPLE'S REPUBLIC OF CHINA
Prof. J.A.C. Cabral, Instituto Superior Tecnico, PORTUGAL
Dr. O. Petrus, AL I CUZA Univ., ROMANIA
Dr. J. de Villiers, Fusion Studies, AEC, S. AFRICA
Prof. M.A. Hellberg, Univ. of Natal, S. AFRICA
Prof. D.E. Kim, Pohang Inst. of Sci. & Tech., SO. KOREA
Prof. C.I.E.M.A.T, Fusion Division Library, SPAIN
Dr. L. Stenflo, Univ. of UMEA, SWEDEN
Library, Royal Inst. of Technology, SWEDEN
Prof. H. Wilhelmson, Chalmers Univ. of Tech., SWEDEN
Centre Phys. Des Plasmas, Ecole Polytech, SWITZERLAND
Bibliotheek, Inst. Voor Plasma-Fysica, THE NETHERLANDS
Asst. Prof. Dr. S. Cakir, Middle East Tech. Univ., TURKEY
Dr. V.A. Glukhikh, Sci. Res. Inst. Electrophys.I Apparatus, USSR
Dr. D.D. Ryutov, Siberian Branch of Academy of Sci., USSR
Dr. G.A. Eliseev, I.V. Kurchatov Inst., USSR
Librarian, The Ukr.SSR Academy of Sciences, USSR
Dr. L.M. Kovrizhnykh, Inst. of General Physics, USSR
Kernforschungsanlage GmbH, Zentralbibliothek, W. GERMANY
Bibliothek, Inst. Für Plasmaforschung, W. GERMANY
Prof. K. Schindler, Ruhr-Universität Bochum, W. GERMANY
Dr. F. Wagner, (ASDEX), Max-Planck-Institut, W. GERMANY
Librarian, Max-Planck-Institut, W. GERMANY
Prof. R.K. Janev, Inst. of Physics, YUGOSLAVIA

DATE FILMED

8 / 19 / 93

END